2016

Structure and magnetism of new rare- earth-free intermetallic compounds: Fe3+xCo3−xTi2 (0 ≤ x ≤ 3)

Balamurugan Balamurugan

Bhaskar Das

Manh Cuong Ngyuen

Xiaoshan Xu

Jie Zhang

See next page for additional authors

Authors

Balamurugan Balamurugan, Bhaskar Das, Manh Cuong Ngyuen, Xiaoshan Xu, Jie Zhang, Xiaozhe Zhang, Yaohua Liu, Ashfia Huq, Shah R. Valloppilly, Yunlong Jin, Cai-Zhuang Wang, Kai-Ming Ho, and David J. Sellmyer

APL Materials

Structure and magnetism of new rare-earth-free intermetallic compounds: $Fe_{3+x}Co_{3-x}Ti_2$ ($0 \leq x \leq 3$)

Cite as: APL Mater. 4, 116109 (2016); https://doi.org/10.1063/1.4968517
Submitted: 19 September 2016 . Accepted: 26 October 2016 . Published Online: 28 November 2016

Balamurugan Balasubramanian, Bhaskar Das, Manh Cuong Nguyen, Xiaoshan Xu, Jie Zhang, Xiaozhe Zhang, Yaohua Liu, Ashfia Huq, Shah R. Valloppilly, Yunlong Jin, Cai-Zhuang Wang, Kai-Ming Ho, and David J. Sellmyer

Structure and magnetism of new rare-earth-free intermetallic compounds: $Fe_{3+x}Co_{3-x}Ti_2$ ($0 \leq x \leq 3$)

Balamurugan Balasubramanian,[1,2,a] Bhaskar Das,[1,2] Manh Cuong Nguyen,[3,4] Xiaoshan Xu,[1,2] Jie Zhang,[4,5] Xiaozhe Zhang,[1,2] Yaohua Liu,[6] Ashfia Huq,[7] Shah R. Valloppilly,[1] Yunlong Jin,[1,2] Cai-Zhuang Wang,[3,4] Kai-Ming Ho,[3,4] and David J. Sellmyer[1,2,a]

[1]*Nebraska Center for Materials and Nanoscience, University of Nebraska, Lincoln, Nebraska 68588, USA*
[2]*Department of Physics and Astronomy, University of Nebraska, Lincoln, Nebraska 68588, USA*
[3]*Ames Laboratory, US Department of Energy, Ames, Iowa 50011, USA*
[4]*Department of Physics and Astronomy, Iowa State University, Ames, Iowa 50011, USA*
[5]*Key Laboratory of Material Physics, Institute of Solid State Physics, Chinese Academy of Sciences, Hefei 230031, People's Republic of China*
[6]*Quantum Condensed Matter Division, Oak Ridge National Laboratory, Oak Ridge, Tennessee 37831, USA*
[7]*Chemical and Engineering Materials Division, Oak Ridge National Laboratory, Oak Ridge, Tennessee 37831, USA*

(Received 19 September 2016; accepted 26 October 2016; published online 28 November 2016)

We report the fabrication of a set of new rare-earth-free magnetic compounds, which form the $Fe_3Co_3Ti_2$-type hexagonal structure with P-6m2 symmetry. Neutron powder diffraction shows a significant Fe/Co anti-site mixing in the $Fe_3Co_3Ti_2$ structure, which has a strong effect on the magnetocrystalline anisotropy as revealed by first-principle calculations. Increasing substitution of Fe atoms for Co in the $Fe_3Co_3Ti_2$ lattice leads to the formation of $Fe_4Co_2Ti_2$, Fe_5CoTi, and Fe_6Ti_2 with significantly improved permanent-magnet properties. A high magnetic anisotropy (13.0 Mergs/cm^3) and saturation magnetic polarization (11.4 kG) are achieved at 10 K by altering the atomic arrangements and decreasing Fe/Co occupancy disorder.

There have been intensive global theoretical and experimental efforts towards the development of alternative permanent-magnet materials, free of strategically vulnerable rare-earth elements or expensive Pt, due to their growing demand in a wide range of applications such as hard-disk drives, spintronics, hybrid vehicles, wind turbines, home appliances, and biomedical devices.[1–5] One focus is on new Co- and/or Fe-rich transition-metal compounds having non-cubic crystal structures, since they have potential to exhibit high magnetocrystalline anisotropy constant ($K_1 \geq 10$ Mergs/cm^3) and saturation magnetic polarization ($J_s \geq 10$ kG, $J_s = 4\pi M_s$, M_s = saturation magnetization), both being essential for permanent-magnet applications.[6–11] However, there exist two challenges: First, new compounds often require high crystallization temperatures and/or are stable only at above 1000 °C.[8,11] Second, it is challenging to determine the complete crystal structure of new magnetic compounds, including atomic arrangements, which have strong effects on their magnetic anisotropy and magnetization. Additionally, such structural information can provide new insights to achieve desired magnetic properties by modifying atomic arrangements via further substitutional alloying.

$Fe_3Co_3Ti_2$ is an intriguing and a recently discovered magnetic compound, which crystallizes into a hexagonal structure with P-6m2 symmetry with a unit cell of 24 atoms (3 f.u.), as schematically shown in Fig. 1(a).[12] This compound exhibits an appreciable Curie temperature $T_c \approx 550$ K, but its

[a]Electronic addresses: bbalasubramanian2@unl.edu and dsellmyer@unl.edu

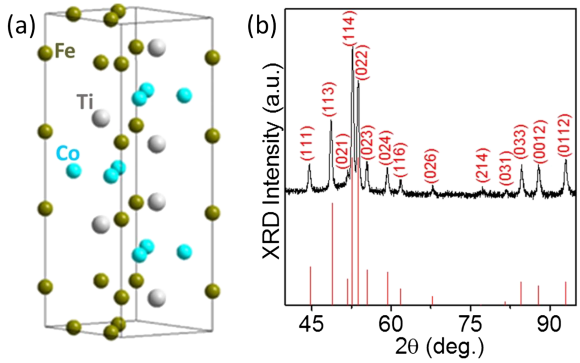

FIG. 1. (a) A Schematic of a hexagonal crystal-structure with *P*-6*m*2 symmetry. (b) Experimental x-ray diffraction pattern of the $Fe_3Co_3Ti_2$ alloy. The standard x-ray diffraction peak positions and relative intensities are marked as vertical lines.

experimentally observed values of magnetic polarization and anisotropy are only moderate from the view point of permanent-magnet applications, i.e., $J_s = 8.6$ kG and $K_1 = 6.0$ Mergs/cm^3.[12] A genetic algorithm (GA) search and subsequent first-principle calculations predict that a Fe/Co disorder has strong effects on the anisotropy of $Fe_3Co_3Ti_2$. In this study, we show direct evidence for Fe/Co antisite disorder in the $Fe_3Co_3Ti_2$ structure using neutron powder diffraction (NPD). We have further modified the atomic arrangements in the structure by gradually replacing Co with Fe to obtain new magnetic compounds $Fe_4Co_2Ti_2$, Fe_5CoTi_2, and Fe_6Ti_2 with more promising permanent-magnet properties.

$Fe_{3+x}Co_{3-x}Ti_2$ ($0 \le x \le 3$) alloys were fabricated using a conventional arc-melting method followed by a melt-spinning process. In brief, arc-melted alloys having homogeneous mixing and desired compositions were made into nanocrystalline ribbons via rapid quenching from the melt using the melt-spinning process with a wheel speed of 57 m/s. This non-equilibrium process is advantageous in forming new crystal structures and metastable compounds and is described elsewhere.[12] The composition of the melt-spun ribbons was measured using energy dispersive x-ray spectroscopy (EDS) on different locations of the ribbons including free and wheel contacted surfaces and the results show reasonably uniform compositional-distribution. The structural properties were investigated using x-ray diffraction measurements (XRD) with a Rigaku D/Max-B x-ray diffractometer using Co K_α radiation with a wavelength of 1.7903 Å. We also have carried out NPD measurements for $Fe_3Co_3Ti_2$ alloy at beam line POWGEN, Spallation Neutron Source at Oak Ridge National Laboratory. For XRD and NPD measurements, the melt-spun ribbons were mechanically ground into fine powders, and thus the results yield crystal structure representative of the ribbon samples. A superconducting quantum-interference device (SQUID) magnetometer and physical property measurement system (PPMS) were used to measure the magnetic properties. Transmission electron microscopy (TEM) measurements were carried out to investigate the microstructure of the melt-spun samples using a FEI Tecnai Osiris scanning transmission electron microscope.

A GA search is employed for the parent compound $Fe_3Co_3Ti_2$ to find low-energy crystal structures of the new compounds. We used the unit cell parameters determined from the experimental XRD data and an empirical potential, described by the embedded atom method (EAM), to relax the candidate structures to the local minima.[13–16] The atomic structure of $Fe_{3+x}Co_{3-x}Ti_2$ compounds with $1 \le x \le 3$ is obtained by replacing a fraction Co with Fe in $Fe_3Co_3Ti_2$. Spin-polarized density functional theory (DFT) simulations were performed to calculate the magnetocrystalline anisotropy and magnetic moments for these low-energy structures using the Vienna *ab initio* simulation package (VASP), version 5.3.[17] The Ceperley–Alder local density approximation (LDA) and projector-augmented wave (PAW) methods were adopted for these calculations.[18–20]

Figure 1(b) shows the experimental XRD pattern of the $Fe_3Co_3Ti_2$ compound. The measured XRD peak positions and intensities are in good agreement with those of the standard diffraction lines corresponding to the hexagonal *P*-6*m*2 structure (vertical lines in Fig. 1(b)). Note that the calculated diffraction lines are from the simulated XRD pattern. Since the x-ray scattering factors of Fe and Co

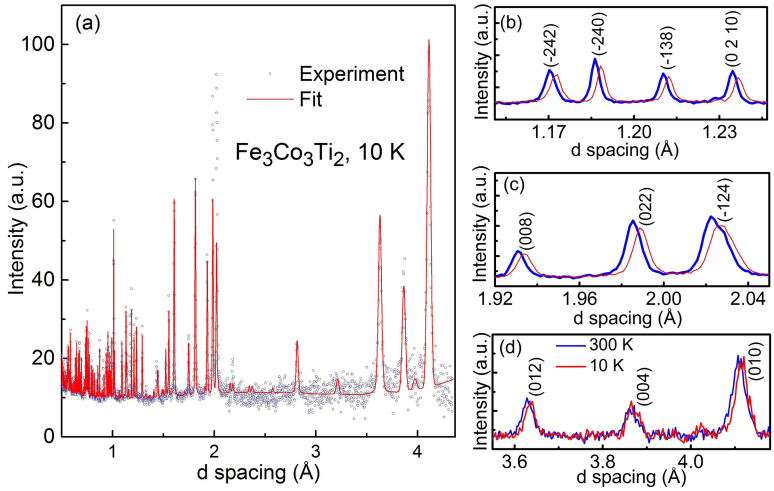

FIG. 2. (a) Powder neutron diffraction spectrum of the $Fe_3Co_3Ti_2$ alloy measured at 10 K (dots) and the fit (line at the top), using the hexagonal *P*-6*m*2 structure. (b)-(d) The Bragg diffraction profiles for the $Fe_3Co_3Ti_2$ alloy measured at 300 and 10 K in different range of *d* spacing.

are very similar for Co K_α radiation, it is not feasible to quantify the Fe/Co antisite disorder from XRD. However, there is a high contrast between the Fe and Co neutron nuclear scattering lengths. In order to determine the antisite disorder between Fe/Co, we have carried out NPD measurements on the $Fe_3Co_3Ti_2$ alloy. The NPD spectrum measured at 10 K for $Fe_3Co_3Ti_2$ alloy is shown as a dotted curve in Fig. 2(a). We have fitted the NPD spectra for the *P*-6*m*2 hexagonal structure by the Rietveld method using the Fullprof Suite[21–23] and the fitted data are shown as a solid curve in Fig. 2(a). As shown in Table I, a significant Fe/Co antisite disorder has been found from the best fit. The fitting also yields the lattice parameters a = 4.743 Å and c = 15.444 Å for $Fe_3Co_3Ti_2$ at 10 K, which agree well with those determined from the XRD pattern (a = 4.754 Å and c = 15.471 Å at 300 K).

Note that even for the best fit, the experimental NPD pattern measured at 10 K shows obvious differences in some peak intensities from the simulated one, as shown in Fig. 2(a). This is because the magnetic scattering contribution has not been considered in the model. We carried out temperature-dependent NPD on the isomorphic $Fe_3Co_3Nb_2$, including both the ferromagnetic and the paramagnetic phases (not shown);[24] the analysis also indicates significant anti-site mixings similar to those in Table I, regardless of whether the magnetic contributions are taken into account. Figures 2(b)–2(d) display the NPD patterns of $Fe_3Co_3Ti_2$ measured at 10 and 300 K, which show only a subtle difference in the scattering peak intensities between 10 and 300 K. Besides the peak shift due to the thermal expansion, for peaks of large d spacing (Fig. 2(d)), the diffraction intensity barely changes; for peaks of smaller d spacing (Figs. 2(b) and 2(c)), the intensity changes are more obvious. The origin of such dependence of the intensity change on the d spacing is typically thermal fluctuation of

TABLE I. The observed Fe/Co antisite disorder in the $Fe_3Co_3Ti_2$-type hexagonal structure with *P*-6*m*2 from the Rietveld method. The numbers in the table are the site occupations.

Sites/Wyckoff position	Atom species	Occupancy
Fe1/2g (0, 0, 0.124)	Fe/Co	0.6/0.4 ± 0.05
Fe2/2g (0, 0, 0.622)	Fe/Co	0.6/0.4 ± 0.1
Fe3/2h (1/3, 2/3, 0.133)	Fe/Co	0.2/0.8 ± 0.1
Fe4/3j (0.171, 0.829, 0)	Fe/Co	0.5/0.5 ± 0.1
Co1/6n (0.830, 0.170, 0.753)	Co/Fe	0.5/0.5 ± 0.05
Co2/3k (0.169, 0.831, 1/2)	Co/Fe	0.3/0.7 ± 0.05

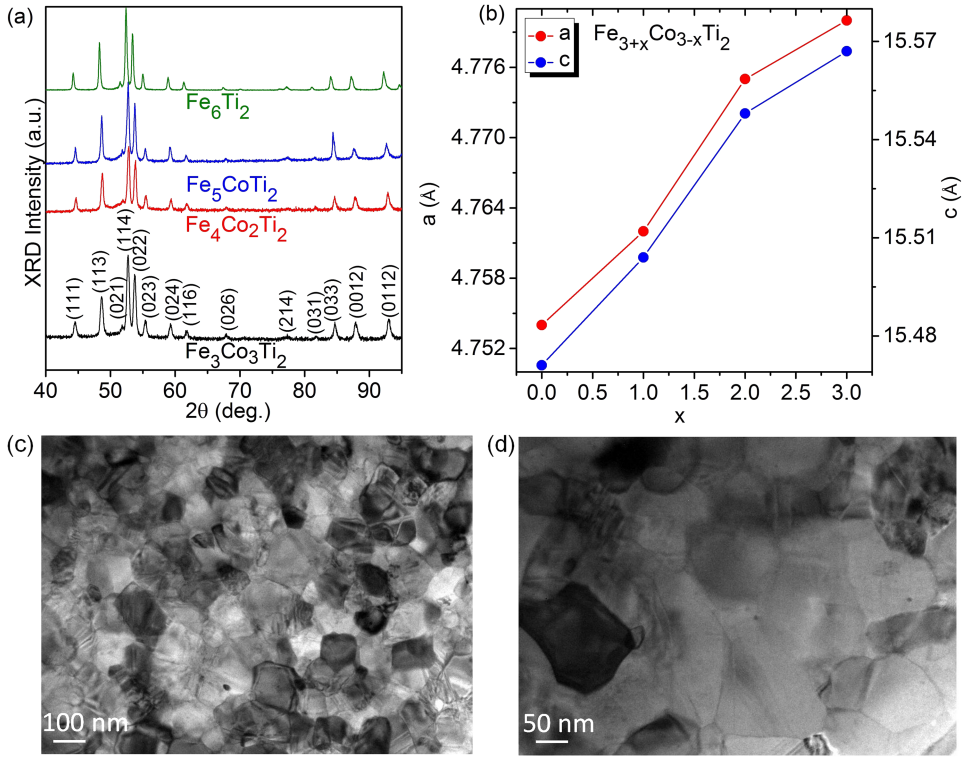

FIG. 3. (a) X-ray diffraction patterns and (b) lattice constants '*a*' and '*c*' measured for $Fe_{3+x}Co_{3-x}Ti_2$ alloys. TEM images of the Fe_6Ti_2 alloy measured at different magnifications are shown in (c) and (d), respectively.

atomic positions.[25] Therefore, there is no apparent change of magnetic diffractions between 10 and 300 K, in good agreement with the temperature dependence of the magnetization measurements (not shown here) and the high $T_c \approx 550$ K.

Motivated by this result, we have studied Fe-rich $Fe_{3+x}Co_{3-x}Ti_2$ alloys ($0 \le x \le 3$), aiming at reducing the Fe/Co antisite disorder and better magnetic properties. It is obvious that there is no Fe/Co antisite disorder for the end alloy, Fe_6Ti_2 (x = 3). Figure 3(a) shows the XRD patterns of $Fe_{3+x}Co_{3-x}Ti_2$ alloys. The $Fe_4Co_2Ti_2$, Fe_5CoTi_2, and Fe_6Ti_2 compounds show XRD patterns similar to that of the $Fe_3Co_3Ti_2$. This result reveals the formation of the same *P*-6*m*2 hexagonal structure in these new compounds. At the same time, the structural refinement of the XRD patterns using Rietveld fitting yields a small and systematic increase in the lattice parameters "*a*" and "*c*" upon the gradual replacement of Co with Fe atoms in $Fe_{3+x}Co_{3-x}Ti_2$ as shown in Fig. 3(b). The microstructural features in these samples are investigated using TEM measurements. Figures 3(c) and 3(d) show the TEM images of the melt-spun Fe_6Ti_2 ribbon sample measured at two different magnifications. The results show that the grains are densely packed and have sizes in the range of around 100 nm. Note that reasonable contrast differences are seen among different grains and this is due to the fact that those grains have different orientations.

In order to show in detail how the replacement of Co with Fe in $Fe_{3+x}Co_{3-x}Ti_2$ improves the magnetic properties, we consider the Fe_5CoTi_2 compound as a typical example and present its magnetic properties obtained from both experiments and theoretical simulations in detail. Figure 4(a) shows the field-dependent magnetization curves of the Fe_5CoTi_2 compound measured at 300 and 10 K for Fe_5CoTi_2. The hysteresis loops reveal higher coercivities H_c for Fe_5CoTi_2 (0.45 kOe at 300 K and 0.70 kOe at 10 K), as compared to the $Fe_3Co_3Ti_2$ alloy (H_c = 60 Oe and 70 Oe at 300 and 10 K, respectively).

A further analysis of the high-field magnetization curve at 10 K between 30 and 70 kOe (not shown here) yields K_1 = 10.7 Mergs/cm^3 and J_s = 9.6 kG for the Fe_5CoTi_2 alloy, as compared to the $Fe_3Co_3Ti_2$ alloy (K_1 = 6.0 Mergs/cm^3 and J_s = 8.6 kG). These values were determined from

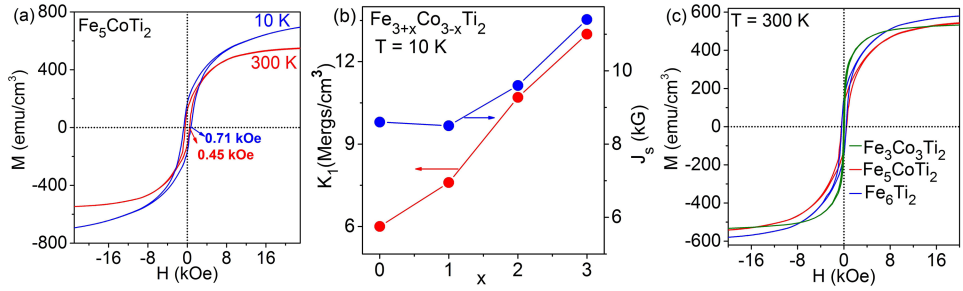

FIG. 4. (a) Field-dependent magnetization curves measured for Fe_5CoTi_2 at 300 and 10 K. (b) Experimental K_1 and J_s values as a function of x in $Fe_{3+x}Co_{3-x}Ti_2$. (c) Room-temperature hysteresis loops of $Fe_3Co_3Ti_2$, Fe_5CoTi_2, and Fe_6Ti_2.

the law-approach-to-saturation method using the equation $M = M_s\,(1 - 4K_1^2/15M_s^2H^2) + \chi H$, where H and χ are the applied magnetic field and high-field magnetic susceptibility, respectively.[26] Note that the term χH in the above equation is only required for fitting the magnetization curves at higher temperatures and very high fields, and thus only the first term was used to determine the magnetic anisotropy and saturation magnetization.[27] Note that J_s is expected to increase for Fe_5CoTi_2 because the Fe moment is higher than the Co moment in the hexagonal $Fe_3Co_3Ti_2$-type structure. The enhanced K_1 is likely due to the lack of Fe/Co disorder in Fe_5CoTi_2.

We also used DFT-LDA calculations to investigate the magnetic properties of Fe_5CoTi_2 compound using the experimental lattice parameters. In order to mimic the effect of disorder in the system, magnetic calculations were performed for about ten Fe_5CoTi_2 structures with random occupation of Fe and Co by swapping the positions of some Fe and Co atoms in the P-6m2 structure. The average magnetic moment is calculated to be 20.99 ± 0.67 μ_B/unitcell (8.1 ± 0.3 kG). The average MAE is 18.1 ± 50.6 μeV/atom (2.3 ± 6.4 Mergs/cm^3), showing a very strong dependence of MAE on the specific arrangement of Fe and Co on the lattice sites of the Fe_5CoTi_2 structure. For comparison, the average magnetic moment and MAE of $Fe_3Co_3Ti_2$ from our current calculations are 17.08 $\pm$ 1.03 μ_B/unitcell (6.6 ± 0.4 kG) and -14.8 ± 27.3 μeV/atom (-1.9 ± 3.5 Mergs/cm^3), respectively. These results show an improvement of magnetic properties of Fe_5CoTi_2 over $Fe_3Co_3Ti_2$.

Note that our DFT calculations are performed for single crystals, whereas the experimental samples are polycrystalline. In addition, the experimental samples can also have real-structure features such as various types of defects, strains, or nano-grains. Although our DFT calculations include some site disorder, the effects of other real-structure features such as the size, shape, and the boundaries of the grains on magnetic properties have not been considered in the calculations. Therefore the results from the DFT calculations only provide an insight into the trend of magnetic anisotropy and magnetization as a function of composition. The theoretical trend agrees with the experimentally observed increase of K_1 and J_s for Fe_5CoTi_2 as compared to $Fe_3Co_3Ti_2$. Experimental results also indicate the improvement of magnetic properties for other compounds as shown in Fig. 4(b), which shows the measured K_1 and J_s at 10 K for $Fe_{3+x}Co_{3-x}Ti_2$ as a function of x. K_1 and J_s values were observed to be maximum for Fe_6Ti_2 ($K_1 = 13.0$ Mergs/cm^3 and $J_s = 11.8$ kG). At 300 K, these values were determined as $K_1 = 10.2$ Mergs/cm^3 and $J_s = 7.9$ kG for Fe_6Ti_2 and $K_1 = 7.6$ Mergs/cm^3 and $J_s = 7.3$ kG for Fe_5CoTi_2. While the hysteresis loops measured at 300 K for Fe_6Ti_2 and Fe_5CoTi_2 show improved coercivities as compared to that of $Fe_3Co_3Ti_2$ (Fig. 4(c)), these values are much lower for permanent-magnet applications.

Coercivity is an extrinsic property of magnetic materials, but it is determined by a combination of intrinsic magnetic properties and various nanostructural features. According to Stoner–Wohlfarth model, the coercivity of an anisotropic (uniaxially aligned) magnetic material should be ideally equivalent to anisotropy field, i.e., $H_c = H_A = 2K_1/M_s$, and thus the ideal room-temperature Stoner–Wohlfarth coercivities are about 32 kOe and 26 kOe for Fe_6Ti_2 and Fe_5CoTi_2, respectively. However, in real experiments, H_c is substantially decreased often by more than one order of magnitude from H_A due to the exchange interactions between the magnetic grains and the presence of defects or nanoscale imperfections.[28–30] Note that bulk magnets are often composed of at least 10% of non-magnetic phase to achieve appreciable coercivities by mitigating the inter-grain exchange interactions.[29] For

example, a Nd-rich grain boundary phase is required to obtain a coercivity of about 20%-30% of H_A in $Nd_2Fe_{14}B$-based permanent magnets.[30] In the present study, the TEM results, shown in Figs. 3(c) and 3(d), reveal that the melt-spun ribbon samples are composed of densely packed grains, which are expected to facilitate the inter-grain exchange interactions and subsequently reduce the coercivities in these materials. However, the appreciable intrinsic permanent-magnet properties of Fe_5CoTi_2 and Fe_6Ti_2 reported in this study will stimulate further research towards developing high coercivity in these materials. This can be achieved via controlling the exchange interactions between the magnetic grains by separating them using a very thin non-magnetic layer and obtaining the crystallographic alignment of the easy magnetization axes.

In conclusion, a rapid-quenching process using the melt-spinning method was used to fabricate rare-earth-free magnetic compounds with the $Fe_3Co_3Ti_2$-type hexagonal structure. A combination of experiments and theoretical simulations using a GA search and DFT calculations was used to determine the structure of the new compounds and correlate their magnetic properties with the structural changes. The atomic arrangements in $Fe_{3+x}Co_{3-x}Ti_2$ were tailored by gradually substituting Co atoms with Fe in a series of alloys, including $Fe_4Co_2Ti_2$, Fe_5CoTi_2, and Fe_6Ti_2, which show increasingly improved properties for permanent magnets. For example, for Fe_5CoTi, $K_1 = 10.7$ Mergs/cm^3 and $J_s = 9.6$ kG at 10 K and $K_1 = 7.6$ Mergs/cm^3 and $J_s = 7.3$ kG at 300 K; and for Fe_6Ti_2, $K_1 = 13$ Mergs/cm^3 and $J_s = 11.4$ kG at 10 K and $K_1 = 10.2$ Mergs/cm^3 and $J_s = 7.9$ kG at 300 K. By nanostructuring and easy-axis alignment, H_c can be further increased, and a $(BH)_{max}$ of about 15-32 MGOe might be achieved in the temperature range of 300 K–10 K. Thus, this research may provide new materials as alternative rare-earth-free permanent magnets containing only earth-abundant elements for sustainable clean energy.

Experimental work by B.B., B.D., X.X., S.R.V., and D.J.S. was supported by the National Science Foundation (NSF), Division of Materials Research (DMR), under Award DMREF: SusChEM 1436385. Theoretical research by C.Z.W. and K.M.H. was supported by NSF, DMR, under Award DMREF: SusChEM 1436386. Research at Nebraska was performed in part in the Nebraska Nanoscale Facility, Nebraska Center for Materials and Nanoscience, which is supported by the NSF under Award NNCI: 1542182, and the Nebraska Research Initiative (NRI). Resources at Spallation Neutron Source, a DOE Office of Science User Facility operated by the Oak Ridge National Laboratory, were also used for this research.

[1] D. J. Sellmyer, Nature **420**, 374 (2002).
[2] J. M. D. Coey, Scr. Mater. **67**, 524 (2012).
[3] D. Kramer, Phys. Today **63**(6), 22 (2010).
[4] N. Jones, Nature **472**, 22 (2011).
[5] M. H. Walmer, J. F. Liu, and P. C. Dent, "Current status of permanent magnet industry in the United States," in *Proceedings of 20th International Workshop on Rare Earth Permanent Magnets and Their Applications, 2008* (Greece, 2008), pp. 37–41.
[6] R. Skomski, P. Manchanda, P. Kumar, B. Balamurugan, A. Kashyap, and D. J. Sellmyer, IEEE Trans. Magn. **49**, 3215 (2013).
[7] D. Niarchos, G. Giannopoulos, M. Gjoka, C. Sarafidis, V. Psycharis, J. Rusz, A. Edström, O. Eriksson, P. Toson, J. Fidler, E. Anagnostopoulou, U. Sanyal, F. Ott, L.-M. Lacroix, G. Viau, C. Bran, M. Vazquez, L. Reichel, L. Schultz, and S. Fähler, JOM **67**, 1318 (2013).
[8] B. Balamurugan, B. Das, V. R. Shah, R. Skomski, X. Z. Li, and D. J. Sellmyer, Appl. Phys. Lett. **101**, 122407 (2012).
[9] A. G. Kusne, T. Gao, A. Mehta, L. Ke, M. C. Nguyen, K.-M. Ho, V. Antropov, C.-Z. Wang, M. J. Kramer, C. Long, and I. Takeuchi, Sci. Rep. **4**, 6367 (2014).
[10] A. Makino, P. Sharma, K. Sato, A. Takeuchi, Y. Zhang, and K. Takenaka, Sci. Rep. **5**, 16627 (2015).
[11] B. Balasubramanian, P. Manchanda, R. Skomski, P. Mukherjee, S. R. Valloppilly, B. Das, G. C. Hadjipanayis, and D. J. Sellmyer, Appl. Phys. Lett. **108**, 152406 (2016).
[12] J. Zhang, M. C. Nguyen, B. Balasubramanian, B. Das, D. J. Sellmyer, Z. Zeng, K.-M. Ho, and C.-Z. Wang, J. Phys. D: Appl. Phys. **49**, 175002 (2016).
[13] D. M. Deavon and K. M. Ho, Phys. Rev. Lett. **75**, 288 (1995).
[14] M. Ji, C.-Z. Wang, and K.-M. Ho, Phys. Chem. Chem. Phys. **12**, 11617 (2010).
[15] M. S. Daw and M. I. Baskes, Phys. Rev. B **29**, 6443 (1984).
[16] X. W. Zhou, R. A. Johnson, and H. N. G. Wadley, Phys. Rev. B **69**, 144113 (2004).
[17] G. Kresse and J. Furthmüller, Phys. Rev. B **54**, 11169 (1996).
[18] D. M. Ceperley and B. J. Alder, Phys. Rev. Lett. **45**, 566 (1980).
[19] P. E. Blöchl, Phys. Rev. B **50**, 17953 (1994).
[20] G. Kresse and D. Joubert, Phys. Rev. B **59**, 1758 (1999).
[21] See https://neutrons.ornl.gov/powgen/users for information about POWGEN, a powder diffraction instrument at the Spallation Neutron Source.

[22] J. Rodríguez-Carvajal, Physica B **192**, 55 (1993).
[23] A. Huq, J. P. Hodges, O. Gourdon, and L. Heroux, Z. Kristallogr. **1**, 127 (2011).
[24] X. Xu, X. Zhang, Y. Yin, B. Balasubramanian, B. Das, Y. Liu, A. Huq, and D. J. Sellmyer, "Anti-site mixing and magnetic properties of $Fe_3Co_3Nb_2$ studied by neutron powder diffraction," J. Phys. D.: Appl. Phys. (in press).
[25] L.-M. Peng, G. Ren, S. L. Dudarev and M. J. Whelan, Acta Crystallogr., Sect. A: Found. Crystallogr. **52**, 456–470, (1996).
[26] G. C. Hadjipanayis, D. J. Sellmyer, and B. Brandt, Phys. Rev. B **23**, 3349 (1981).
[27] A. Franco, Jr. and F. C. e Silva, Appl. Phys. Lett. **96**, 172502 (2010).
[28] B. Balasubramanian, B. Das, W.Y. Zhang, R. Skomski, and D.J. Sellmyer, J. Phys.: Condens. Matter **26**, 064204 (2014).
[29] Y. Hirayama, T. Miyake, and K. Hono, JOM **67**, 1344 (2015).
[30] T. G. Woodcock, Y. Zhang, G. Hrkac, G. Ciuta, N. M. Dempsey, T. Schrefl, O. Gutfleisch, and D. Givord, Scr. Mater. **67**, 536 (2012).